AIP | Review of Scientific Instruments

Figuring with subnanometer-level accuracy by numerically controlled elastic emission machining

Kazuto Yamauchi, Hidekazu Mimura, Kouji Inagaki, and Yuzo Mori

Citation: Review of Scientific Instruments **73**, 4028 (2002); doi: 10.1063/1.1510573
View online: http://dx.doi.org/10.1063/1.1510573
View Table of Contents: http://scitation.aip.org/content/aip/journal/rsi/73/11?ver=pdfcov
Published by the AIP Publishing

Figuring with subnanometer-level accuracy by numerically controlled elastic emission machining

Kazuto Yamauchi, Hidekazu Mimura,[a] Kouji Inagaki, and Yuzo Mori
Department of Precision Science and Technology, Graduate School of Engineering, Osaka University, 2-1 Yamada-oka, Suita, Osaka 565-0871, Japan

(Received 25 February 2002; accepted 27 July 2002)

A numerically controlled elastic emission machining (EEM) system has been developed to fabricate ultraprecise optical components, particularly in x-ray optics. Nozzle-type EEM heads, by which a high shear-rate flow of ultrapure water can be generated on the work surface, have been newly proposed to transport the fine powder particles to the processing surface. Using this type of EEM head, the obtainable spatial resolution in figure correction can be changed by selecting the suitable aperture size of the nozzle according to the required spatial frequency. As a result of test figuring, 1 nm level peak-to-valley (p–v) accuracy is achieved throughout the entire spatial wavelength range longer than 0.3 mm. In addition, the microroughness of the processed surface is certified to also be approximately 1 nm (p–v). [DOI: 10.1063/1.1510573]

I. INTRODUCTION

Recently, ultraprecise figuring technology is in great demand in many scientific fields. Particularly in third-generation synchrotron radiation sources or next-generation extreme ultraviolet lithography systems, ultraprecise mirrors with figure accuracy higher than nanometer order [peak-to-valley ($p-v$)] are required.[1–3] Currently, many figuring methods are being intensively studied in order to realize the required figure accuracy.[4–8] Computer-controlled polishing (CCP), the principles of which basically originated in Preston's semiempirical theorem,[8] is the most popular figuring method. In this method, small tools such as the small pitch polisher are employed to realize the desired removal depth profile with respect to the premachined surface error height. Tool velocity, dwelling time, and pressure can be employed as the parameters to be controlled in figuring. The dwelling time is selected in many CCP systems[4–6,9] because of the ease of generating numerical data for controlling the tool scan. The tool pressure has also been selected in the multi-tool polishing machine.[7] However, in those systems, figure accuracy of 10 nm ($p-v$) seems to be the achievable limit, because of the difficulty in keeping many kinds of process parameters, such as slurry concentration, temperature, and conditions of the tool surface, constant. The removal rate in practical polishing is set to be 0.001–1 nm/min according to the desired accuracy to be realized.[5,6,9] The volumetric removal rate is related to the tool size. As a result of current technical achievements, the spatial resolution of figuring, which depends on the tool size, is larger than a few millimeters. On the other hand, ion-beam sputtering, which is a dry process, has been developed as a method of computer-controlled figuring. The process parameters, such as gas pressure and ion current, are kept constant more easily than those in the CCP method, so that the expected figuring accuracy is considered to be high compared to that of the CCP method. Currently, the achievable p–v figure error is as small as a few nanometers. However, the two methods described above utilize the mechanical effects in material removal, whereby a crystallographically damaged layer, such as plastically deformed or amorphous layers must be introduced, so they can not be applied in fields such as Bragg diffraction optics in which the crystallographic nature of the polished surfaces is utilized. In contrast, elastic emission machining (EEM) can yield atomically smooth surfaces without introducing any crystallographic damage.[10–12] In this method, chemical phenomena between the surfaces of the work piece and the fine powder particles are utilized.[13,14] One nanometer-level accuracy ($p-v$) can also be achieved as long as the supply rate of the fine powder particles to the work surface is precisely controlled to be constant. The removal rate in EEM directly corresponds to the supply rate of the fine particles that are reactive with the atoms on the work surface.[15] A removal rate of 1 nm/min is obtainable in EEM, which is not so low compared with other figuring methods with nanometer-order accuracy.

The aim of this study is to realize an ultraprecise figuring system having the accuracy of 1 nm ($p-v$) and 0.1 nm [root-mean-square (rms)]. In this study, nozzle-type EEM heads, by which a high shear-rate flow of ultrapure water can be generated on the work surface to transport the fine powder particles, has been newly proposed and incorporated in the designed machine. As a result of the test figuring, 1 nm level accuracy ($p-v$) is achieved throughout the entire spatial wavelength range longer than 0.3 mm. In addition, the microroughness of the processed surface is certified to also be approximately 1 nm ($p-v$).

II. REQUIREMENT OF ENVIRONMENTAL CLEANLINESS

The removal mechanism in EEM is chemical, as mentioned previously, so that the avoidance of the introduction of

[a]Electronic mail: mimura@up.prec.eng.osaka-u.ac.jp

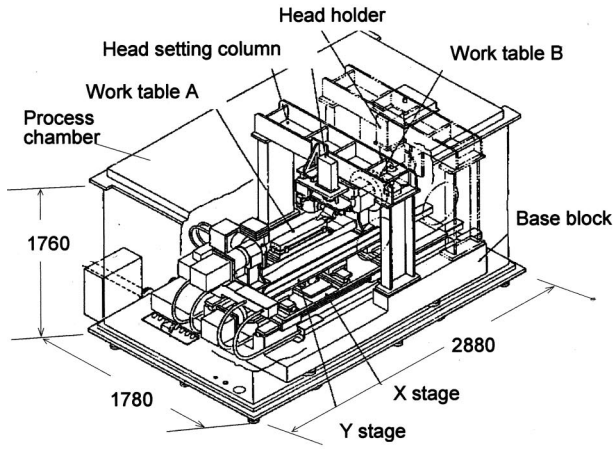

(a)

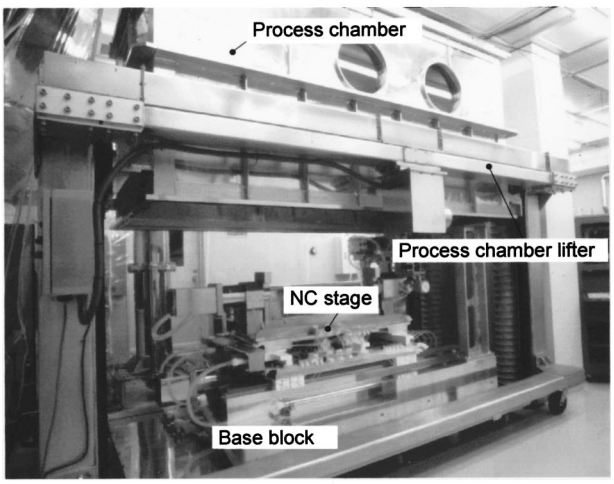

(b)

FIG. 1. Schematic drawing and photograph of EEM apparatus in ultraclean room. Workpiece and a mixture fluid are completely isolated from room atmosphere by a stainless-steel vessel to avoid the oxygen supply. (a) schematic drawing and (b) photograph.

the following two types of impurities is very important in the development of an ultraprecise EEM system. One is organic contamination on the processed surface, which acts as a blocking mask against the chemical reactions utilized in EEM and leads to finished surface microroughness. The other is dissolved oxygen in ultrapure water, which is so active that the processed surface is destructively oxidized. Particularly for the Si substrate, the oxide growth rate may be higher than 1 nm/min, depending on the process conditions.

III. NUMERICALLY CONTROLLED ELASTIC EMISSION MACHINING

A schematic and photograph of the EEM system are shown in Fig. 1. All of the stages are enclosed in the ultrapure water vessel to prevent the introduction of oxygen gas and organic materials such as oil vapor. Two worktables, which are constructed with a common x, y, and θ stage, are installed, as seen in Fig. 2. Worktable A is used for flat, cylindrical, and toroidal x-ray mirrors. The other one is used

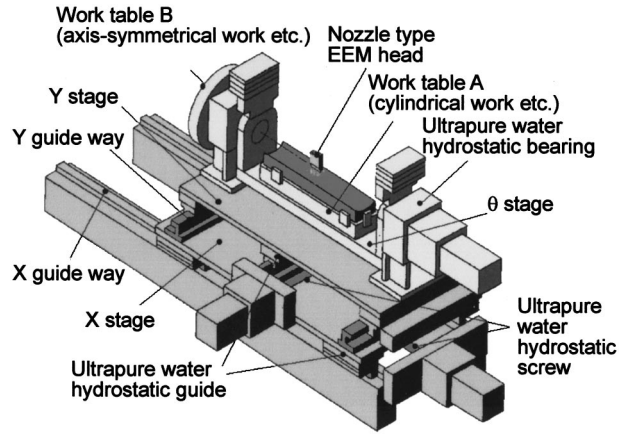

FIG. 2. Schematic view of numerically controlled x, y, θ stages. The guides, bearings, and drive screws are hydrostatically supported by pressurized ultrapure water to avoid metal contact.

for the axisymmetric optical components. The strokes of x and y stages are 600 and 200 mm, respectively. A hydrostatic supporting system utilizing ultrapure water is applied to the guides, bearings, and drive screws of the stages to avoid both organic contaminants from the lubricant and the metallic dust produced as a result of the mechanical friction.

IV. ELASTIC EMISSION MACHINING HEAD

In EEM, the fine powder particles that are reactive with the atoms on the work surface are mixed into the ultrapure water and supplied to the work surface along the streamline of the forced flow. When the surface of the powder particle and the work surface come into contact with each other and then separate, there is an appreciable probability that the atoms of one surface will adhere to the other surface. A nozzle-type EEM head has been newly developed to transport the fine powder particles effectively to the work surface. To remove the powder particles which are chemically interacting with the work surface, shear flow with a rate of more than 1

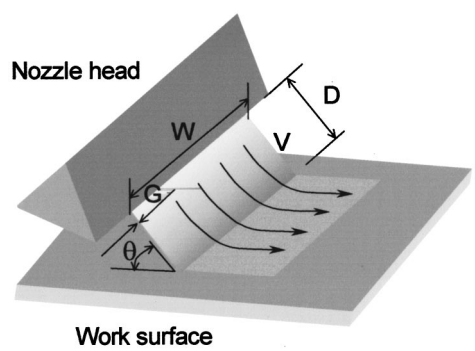

Specifications	
Gap of slit : G	50μm~200μm
Width of slit : W	0.5~20mm
Incident angle : θ	35° ~ 90°
Facing distance : D	1mm~2mm
Initial velocity of fluid : V	~ 100m/s
Pressure	~ 10^7Pa

FIG. 3. Schematic drawing of nozzle-type head and its typical specifications.

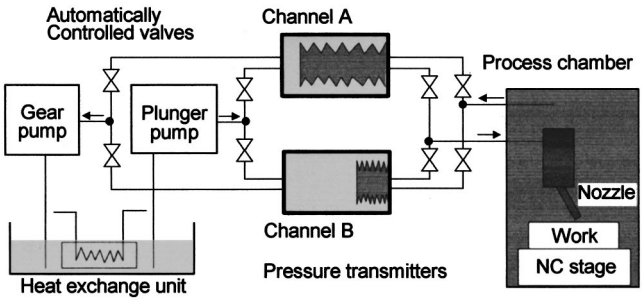

FIG. 4. Schematic diagram of pressurized fluid supply system. The mixture fluid, which is composed of ultrapure water and fine powder particles, can be pressurized without any increase of the concentration of impurities such as dissolved oxygen and organic materials.

m/s μm is required. The head can easily satisfy this requirement. A schematic and typical specifications are shown in Fig. 3. The facing distance, which is about 1 mm, is so large that the removal rate is not sensitive to the gap fluctuation due to vibrations or temperature changes. The aperture size of the slit is a very important parameter in figuring properties, because it governs the size of the processing area and affects the spatial resolution of figuring. The slit size should be selected according to the desired spatial resolution.

An apparatus for transmitting pressure to the mixture fluid is shown in Fig. 4. It is composed of two channels which are alternately operated by automatically controlled valves to supply the pressurized fluid continuously to the nozzle head. In this apparatus, the mixture fluid is charged into the inner area of the bellows by the suction of the gear pump, and then pressurized by the tap water forced into the outer area of the bellows by the plunger pump. The mixture fluid is completely isolated from the tap water so that the pressurized mixture fluid can be kept sufficiently clean.

To test the performance of the EEM head, atomic force microscopy (AFM) observations of EEM-processed surfaces were carried out. The measured profiles of as-received and EEM-processed surfaces are shown in Figs. 5(a) and 5(b), respectively. The microroughness of the preprocessed surface was 2.47 nm $(p-v)$ [0.21 nm (rms)]. In contrast, that of the EEM-processed surface is drastically improved to 1.01 nm $(p-v)$ [0.12 nm (rms)]. In addition, removal volumes of ten independent stationary spots were compared over a period of 100 h to evaluate the stability of the removal rate. The operation parameters and results are shown in Table I and Fig. 6, respectively. The removal rate is confirmed to be stable within a few percent. Figure 7 shows the relationship between the dwelling time and removal depth. The relationship is exactly linear. These results indicate the applicability of the nozzle-type EEM head to numerically controlled figuring.

TABLE I. Experimental conditions.

Work material	Quartz glass
Powder particle	0.1 μm ϕSiO_2
Fluid concentration	10 vol.%
Dwelling time	15 min
Nozzle head conditions	
Aperture size	10 mm×200 μm
Incident angle	90°
Initial fluid velocity	30 m/s

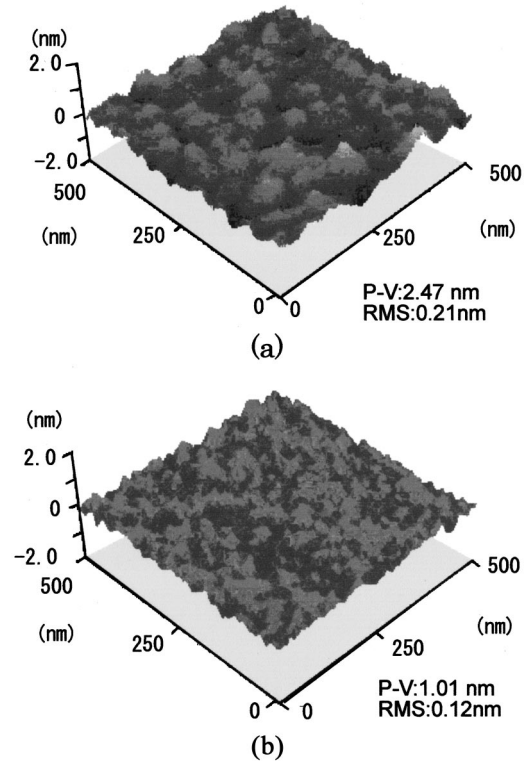

FIG. 5. AFM observation of preprocessed and EEM-processed Si(001) surfaces. Observed area is 500 nm×500 nm: (a) preprocessed surface and (b) EEM-processed surface.

V. NUMERICAL CONTROL SYSTEM

Figuring is performed by scanning the head in the area to be machined at a suitable speed, as shown in Fig. 8. The software used for the calculation of the scanning speed based on the rms-figure-error-minimum algorithm was coded here. The thickness to be removed $M(r_1)$ is calculated from the preprocessed and the required surface profiles at sampling point r_1. The square sum of the figure errors of the finished surface is expressed as

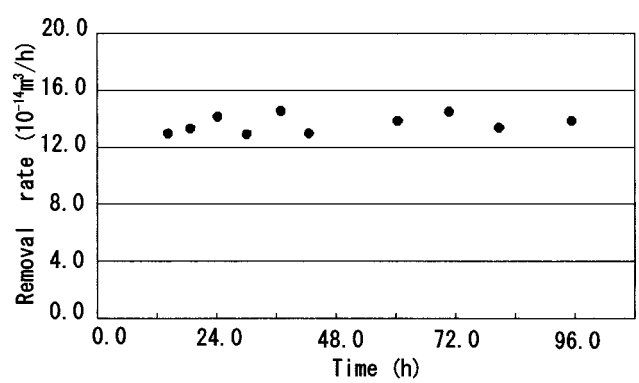

FIG. 6. Reproducibility of removal rate. Removal volumes of the stationary spots are measured independently for 100 h. The fluctuation is kept smaller than a few percent.

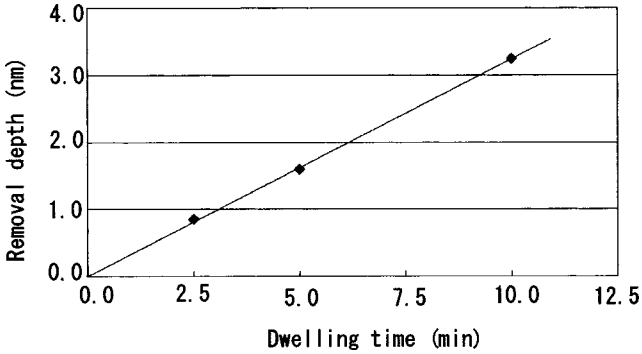

FIG. 7. Linearity between stock removal and dwelling time of EEM head. High linearity is very important for precise figure correction and is easily realized with the EEM head.

$$E=\sum_{i}^{m}\left\{M(r_i)-\sum_{j}^{n}N_j(r_i)\cdot t_j\right\}^2, \tag{1}$$

where $N_j(r_i)$ is the depth to be removed at point r_1 by the processing at point r_j for a unit time and t_j is the dwelling time to be calculated at the point r_j. Optimized t_j ($j=1,2,3,\ldots,m$) is obtained from

$$\frac{\partial E}{\partial t_j}=0 \quad (j=1,2,3,\ldots n). \tag{2}$$

The scanning rate of the EEM head is proportional to the inverse of the dwelling time t_j. The figure error (rms) of the processed surface can be minimized by this algorithm.

VI. FIGURING PERFORMANCE

In order to evaluate the performance of figure correction, two experiments of figuring are carried out. One is a test of spatially long-range correction of the figure error. Another is that of spatially high-resolution figuring. The figure measurement ability limits the figuring performance so that the following two types of interferometers are employed in this study. One is a Fizeau interferometer with the reference plate calibrated by the three references method, which has nanometer accuracy in the long spatial wavelength range (<10 mm). The other is a Michelson microscopic interferometer with a system error smaller than 0.1 nm (rms) in the area of view of 5 mm square. They are applied for figure testing according to both the required area of view and the spatial resolution. Experimental parameters are shown in Table II. Figures 9(a) and 9(b) show the stationary spot profiles obtained using heads with the slit aperture sizes of 200 μm×10 mm and 200μm×1 mm, respectively. The larger spot is suitable for high-speed and relatively low spatial resolution figuring. In contrast, the smaller one is suitable for figuring in the short-wavelength range close to the submillimeter level.

Preprocessed and processed surface profiles by a head with the slit aperture sizes of 200 μm×10 mm (test A) are shown in Figs. 10(a) and 10(b), respectively. The size of the processed area is 30 mm×30 mm. Figure errors before and

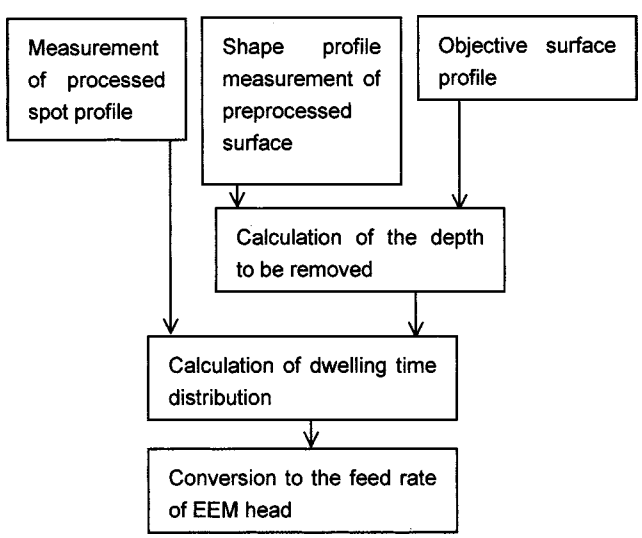

FIG. 8. Procedures for numerically controlled EEM figuring. Premachined surface profile is measured in constant room temperature. Thickness to be removed is calculated and converted to the distribution of the dwelling time.

TABLE II. Process parameters and conditions.

	Test A	Test B
Work material	Quartz glass	Si
Powder particle	0.1 μm^{ϕ} SiO_2	2.0 μm^{ϕ} SiO_2
Fluid concentration	10 vol%	10 vol%
Processed area $X\times Y$	25 mm×21 mm	4 mm×4 mm
Feed direction	Y	Y
Feed rate	~200 mm/min	~200 mm/min
Distance between neighboring feed lines ΔX	10 μm	10 μm
Total processing time	16 h	11 h
Nozzle head conditions		
Aperture size	10 mm×200 μm	1 mm×200 μm
Incident angle	35°	35°
Initial fluid velocity	30 m/s	30 m/s

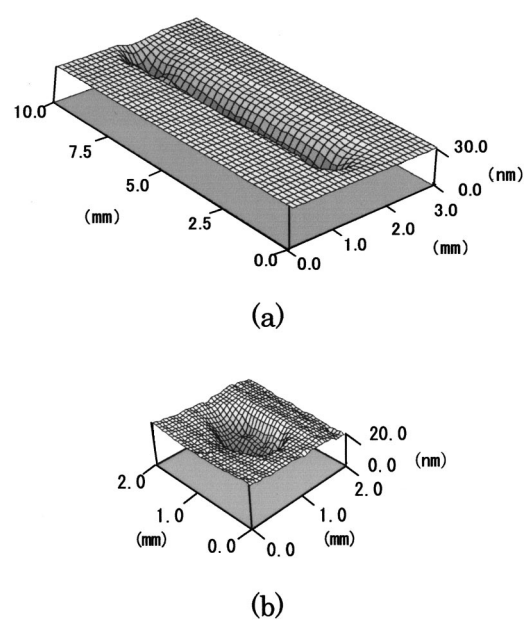

FIG. 9. Stationary spot profiles obtained using nozzle-type EEM heads. The profiles are measured using a microscopic interferometer with the area of view of 5 mm square. The profile of the larger spot is obtained by the stitching several shots of the microscopic interferometer images: (a) slit aperture size of 200 μm×10 mm and (b) slit aperture size of 200 μm×1 mm.

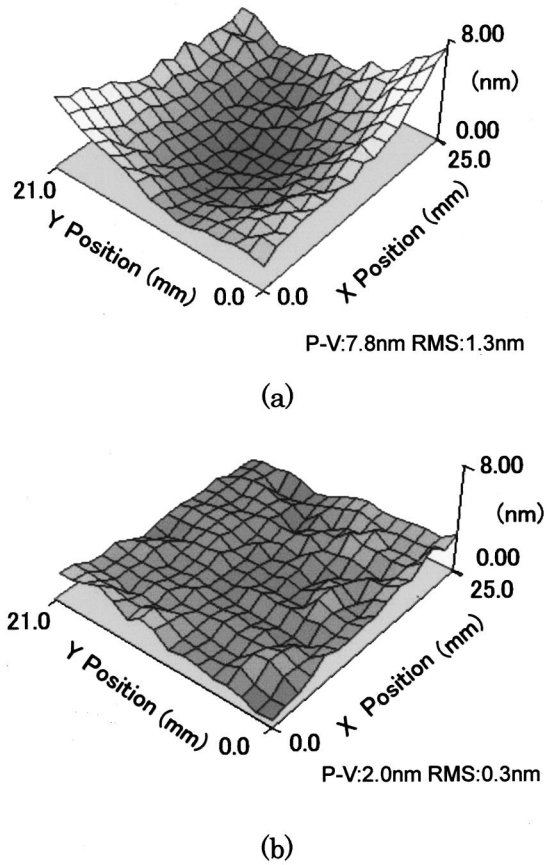

FIG. 10. The preprocessed and processed surface profiles measured using Fizeau interferometer. Figure errors before and after figure correction are given in the figure as both $p-v$ and rms expressions: (a) preprocessed surface profile and (b) processed surface profile.

after figure correction are 7.8 nm $(p-v)$ [1.3 nm (rms)] and 2.0 nm $(p-v)$ [0.30 nm (rms)], respectively. The typical line profiles of the predicted and figured surfaces are compared in Fig. 11. These two profiles are found to be in good agreement with accuracy better than 1 nm $(p-v)$. Figure 12 shows power spectral density (PSD) curves. The nozzle head with the slit aperture size of 200 μm$\times$10 mm is found to realize the spatial resolution of 3 mm. Figure 13 shows the surface profiles before and after the figure correction in 4 mm$\times$4 mm area figuring (test B). Figure errors before and after figure correction are 3.2 nm $(p-v)$ [0.32 nm (rms)] and 0.98 nm $(p-v)$ [0.14 nm (rms)], respectively. Figure 14 shows the comparison between the line profiles of the pre-

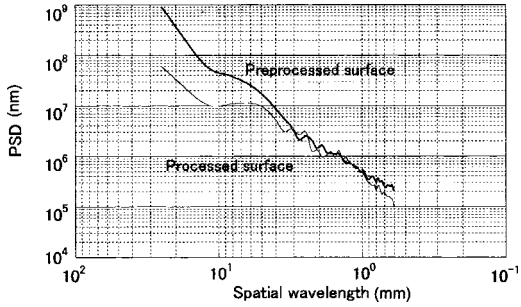

FIG. 12. PSD curves of preprocessed and processed surfaces.

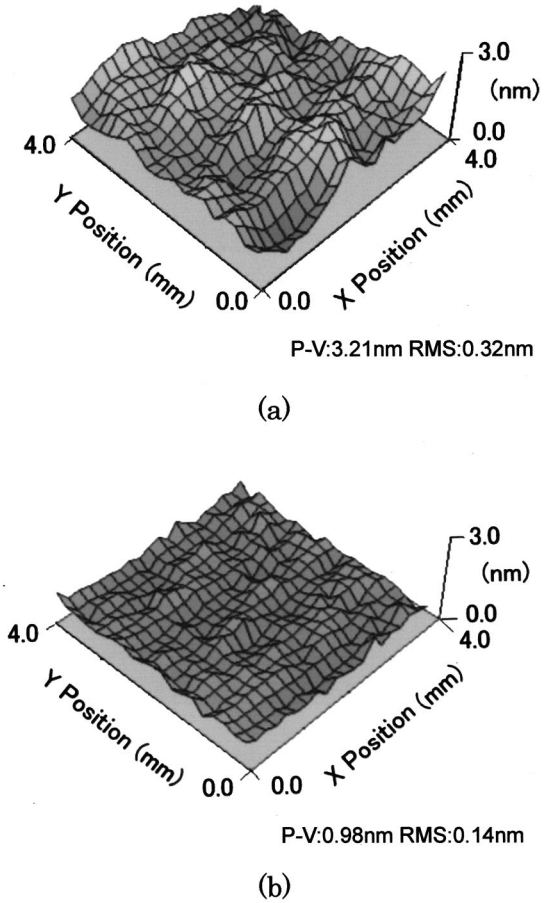

FIG. 13. Preprocessed and processed surfaces profiles measured using Michelson microscopic interferometer. Figure errors before and after figure correction are given in the figure as both $p-v$ and rms expressions: (a) preprocessed surface profile and (b) processed surface profile.

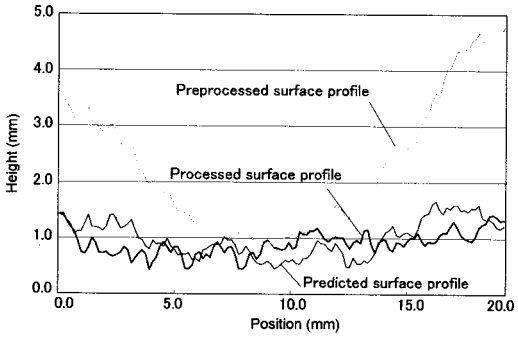

FIG. 11. Comparison between typical line profiles of preprocessed, predicted, and processed surfaces.

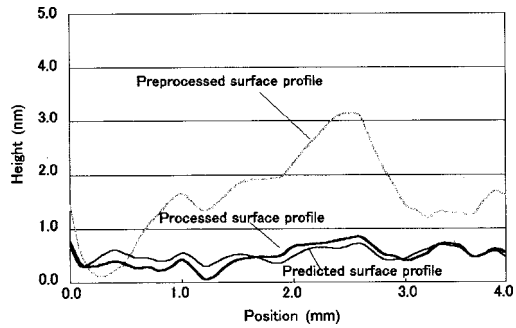

FIG. 14. Typical line profiles of preprocessed, predicted, and processed surfaces.

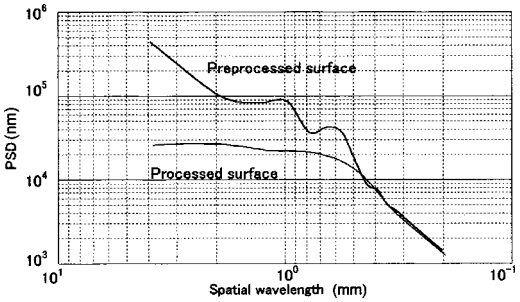

FIG. 15. PSD curves of preprocessed and processed surfaces.

dicted and figured surfaces. They are also in good agreement with accuracy better than 1 nm $(p-v)$. In addition, spatial resolution higher than 0.3 mm is seen to be achieved from the PSD curves shown in Fig. 15.

The numerically controlled EEM system, which has been developed here, is concluded to enable ultraprecise figuring with both height accuracy close to 1 nm $(p-v)$ and spatial resolution higher than 0.3 mm. The accuracy can be considered to be promising for next-generation x-ray optics.

VII. DISCUSSION

A numerically controlled EEM was developed to fabricate ultraprecise optical components, and its figuring performance was evaluated. The results obtained are as follows.

(1) An ultraclean stage system with hydrostatic support by ultrapure water was designed to avoid organic contamination from oil vapors and friction dust, which cause microroughness of the processed surfaces.
(2) The nozzle-type EEM head, newly developed here, was certified to have sufficient stability of the removal rate. The removal rate was found to be constant within a few percent over 100 h. The relationship between the dwelling time and volumetric removal was also certified to be exactly linear.
(3) The processed surface observed by AFM was extremely smooth with the microroughness of 0.12 nm (rms).
(4) A figuring accuracy close to subnanometer $(p-v)$ order was achieved over a spatial wavelength range longer than 0.3 mm.

ACKNOWLEDGMENTS

This work was partially supported by Japan Science and Technology Corporation and by a Grant-in-Aid for COE Research (No. 08CE2004) from the Ministry of Education, Sports, Culture, Science, and Technology.

[1] T. Ishikawa, K. Tamasaku, M. Yabashi, S. Goto, Y. Tanaka, H. Yamazaki, K. Takeshita, H. Kimura, H. Ohashi, T. Matsushita, and T. Ohata, Proc. SPIE **4154**, 1 (2001).
[2] J. Arthur and R. Tatchyn, Proc. SPIE **4143**, 1 (2001).
[3] H. Kinoshita, T. Watanabe, J. Daniel, D. Bajuk, Y. Paltonov, and J. Wood, in *Precision Science and Technology for Perfect Surfaces*, edited by Y. Furukawa, Y. Mori, and T. Kataoka (Japan Society for Precision Engineering, Tokyo, 1999), p. 9.
[4] X. Zhang, J. Yu, Z. Zhang, Q. Wang, and W. Zhang, Opt. Eng. **36**, 3386 (1997).
[5] M. Negishi, M. Ando, A. Deguchi, M. Takimoto, H. Narumi, N. Nakamura, and H. Yamamoto, Proc. SICE'94, (1994), p. 941.
[6] M. Ando, M. Negishi, M. Takimoto, A. Deguchi, N. Nakamura, M. Higomura, and H. Yamamoto, Proc. SPIE **1720**, 22 (1992).
[7] S. Katagiri, M. Ito, H. Yamanashi, E. Seya, and T. Terasawa, JSPE Proceeding of the Second U.S.–Japan Workshop on Soft X-Ray Optics: Technical Challenges (Japan Society for Precision Engineering, Tokyo, 1996), p. 316.
[8] F. W. Preston, J. Soc. Glass Technol. **5**, 42 (1927).
[9] K. B. Becker, in *Precision Science and Technology for Perfect Surfaces*, edited by Y. Furukawa, Y. Mori, and T. Kataoka (Japan Society for Precision Engineering, Tokyo, 1999), p. 51.
[10] Y. Mori, K. Yamauchi, and K. Endo, Precis. Eng. **9**, 123 (1987).
[11] Y. Mori, K. Yamauchi, K. Endo, T. Ide, H. Toyota, K. Nishizawa, and M. Hasegawa, J. Vac. Sci. Technol. A **8**, 621 (1990).
[12] Y. Mori, K. Yamauchi, K. Yamamura, H. Mimura, A. Saito, H. Kishimoto, Y. Sekito, M. Kanaoka, A. Souvorov, M. Yabashi, K. Tamasaku, and T. Ishikawa, Proc. SPIE **4501**, 30 (2001).
[13] Y. Mori, K. Yamauchi, and K. Endo, Precis. Eng. **10**, 24 (1988).
[14] K. Yamauchi, K. Hirose, H. Goto, K. Sugiyama, K. Inagaki, K. Yamamura, Y. Sano, and Y. Mori, Comput. Mater. Sci. **14**, 232 (1999).
[15] Y. Mori, K. Yamauchi, K. Sugiyama, K. Inagaki, S. Shimada, J. Uchikoshi, H. Mimura, T. Imai, and K. Kanemura, in *Precision Science and Technology for Perfect Surfaces*, edited by Y. Furukawa, Y. Mori, and T. Kataoka (Japan Society for Precision Engineering, Tokyo, 1999), p. 207.